OPEN ACCESS

GAVIN PUBLISHERS

Research Article

In Vivo Study of Biodegradable Pure Magnesium Membrane-Guided Bone Regeneration

Yuan Zhao[1†], Man Yang[1†], Yingnan Shang[1], Hong Wei[1], Xueyan Zhang[2], Jingxin Yang[2*], Chengyue Wang[3*]

[1]VIP clinic, Jinzhou Stomatological Hospital, No.28, Section 3, Yichang Road, Guta District,Jinzhou,121000, PR China

[2]College of Robotics, Beijing Union University, No.4 Gongti North Road, Chaoyang District, Beijing, PR China

[3]Department of Prosthodontics, The Stomatological Hospital affiliated with Jinzhou Medical University; No. 49, Section 2, Shanghai Road, Guta District,Jinzhou,121000, PR China

[†]These authors contributed equally

[*]**Corresponding Authors:** Jingxin Yang, College of Robotics, Beijing Union University, No.4 Gongti North Road, Chaoyang District, Beijing, PR China; Chengyue Wang, Department of Prosthodontics, The Stomatological Hospital affiliated with Jinzhou Medical University; No. 49, Section 2, Shanghai Road, Guta District,Jinzhou,121000, PR China.

Abstract

This study explored the use of a pure magnesium-shielding membrane combined with bone graft materials for repairing vertical bone defects in the mandibular canine. The samples were randomized into three groups, and a vertical box-shaped bone defect model was established in the mandibular fourth premolars of the canines. Group A consisted of pure magnesium membranes combined with bone graft materials (n=4); Group B was composed of Bio-Gide collagen membranes combined with bone graft materials (n=4); and Group C served as the control group, consisting only of bone graft materials (n=4).Gross specimens were obtained from the three groups at predetermined time points. Cone beam computed tomography, X-ray microscopy, and histological analysis were used to evaluate the bone repair ability and local soft-tissue biocompatibility of the implanted materials. At 4, 12, and 24 weeks after surgery, the relative bone mineral density of the pure magnesium membrane group was higher than that of both the collagen membrane group and the control group.At 24 weeks after surgery, the pure magnesium membrane had completely degraded; the area of osteogenesis was filled with new bone, and the trabecular bone was thick and dense.No inflammation was observed in either the epithelial layer or the lamina propria of the mucosa. The pure magnesium membrane can guide and control the outline of regenerated bone, better maintaining the space for bone regeneration in larger defects, while also exhibiting good biocompatibility with local soft tissue in the implanted area.

Introduction

Guided Bone Regeneration (GBR) technology is extensively used in clinical applications. GBR membrane technology is applied in implant surgery to address bone defects around the implant, local bone shortages in the anterior teeth areas, and inflammation-induced bone resorption around the implant after implantation. This technology provides a new and effective alternative treatment method, resulting in a significant improvement in the success rate of implant surgery for bone defects [1]. Guided bone regeneration involves placing a barrier membrane between the bone defect and the mucoperiosteal flap to prevent connective tissue cells and epithelium from growing.This protects the bone graft material and provides an isolated space for bones and antigenic cells to grow. The shielding membrane plays an important role in guiding bone regeneration [2]. At present, GBR membranes mainly include non-absorbable (Gore-Tex and pure titanium membranes) and absorbable membranes (collagen and ester-lactide copolymer membranes).Non-absorbable membranes can be designed in various shapes to fit the size and shape of bone defects accurately. In addition, non-absorbable membranes have a strong ability to block soft tissues and can remain in the body for months or even years. However, the clinical applications of non-absorbable membranes are limited because they require a second operation to remove them 6 to 12 months after surgery.The absorbable biofilm will decompose into the tissues over time. If it decomposes too quickly,it may result in incomplete osteogenesis.In addition,the absorbable biofilm has poorer absorbability compared to the metal film and may collapse into the bone defect area, affecting bone formation [3-5].

Can the shielding film possess both the mechanical properties of metal and biodegradability?Magnesium metal has become a popular research topic in the fields of orthopaedics and dental implant materials.Magnesium is a type of degradable metal with both the mechanical properties of metal and biodegradability. The elastic modulus of magnesium metal is closer to that of dense bone in the human body than other metals, and it can alleviate the stress shielding effect better than titanium alloy and stainless steel [6]. Magnesium ions, the degradation product of magnesium, can promote the deposition of calcium phosphate and collagen as well as enhance osteogenic reactions.The magnesium ions on the surface of the material can promote bone cell adhesion.Thus, magnesium and magnesium alloys are more likely to be used as materials for guided bone regeneration membranes [7,8]. Our previous research investigated the issue of matching magnesium metal degradation with bone formation processes under specific physiological conditions, such as those found in alveolar bone [9-11]. Based on prior in-vitro experimental research, we prepared high-purity magnesium membranes to establish and maintain a space for bone regeneration.In vivo animal experiments were conducted to explore the effect of a pure magnesium membrane combined with bone graft material for repairing vertical bone defects in dog mandibles.

Materials and Methods

Materials Characterisations

We used pure magnesium film that was 0.5mm thick (>99.95%) and magnesium nails that were 10mm in length and 2mm in diameter. Half-tapping screws were provided by the Institute of Metals, Chinese Academy of Sciences. The in vitro experiment was partly based on our previous research [12]. Beijing Allgens Medical Science & Technology Co. Ltd produced bone graft materials, which consist mainly of type I collagen and hydroxyapatite.The hydroxyapatite content was $45\pm5\%$. We used a Co-2 cylinder with a diameter of $10mm\pm0.5mm$, a length: $20mm\pm1mm$, a compressive strength of $\geq0.8MPa$, a porosity of 70%-80%, a pore size of(300 ± 250) μm, and a crystal size of 20-50mm. The FDA 510(k) license number is K141725. Bio-Gide membrane is produced by the Swiss company Geistlich and provided by Gesite Trading (Beijing) Co. Ltd.Specifications: The collagen membrane is 25mm in length and 25mm in width, consisting of type I and type III collagens to form a double-layer structure. The outer layer is dense with pore sizes ranging from 0.5-2.0μm, while the inner layer is porous with pore sizes ranging from 30-100μm (Figure 1)**.**
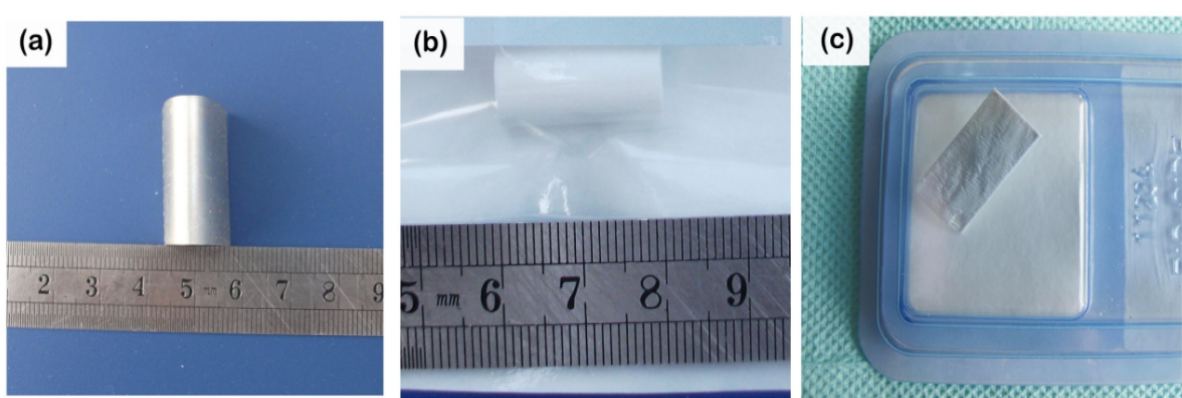
**Figure 1:** Experimental Materials (a) Pure magnesium film;(b) Bone graft materials;(c) Bio-Gide membrane.

In Vivo Study

Animals and Grouping: This in vivo study involved 12 dogs, which were provided by the Experimental Animal Centre at Jinzhou Medical University. The dogs were between 12 and 24 months old, weighed between 15 and 20 kg, and included both males and females. The inclusion criteria were as follows: the animals had complete frontal dental dentition, no chronic periodontal disease or dental caries, normal oral mucosa coloration, and no obvious occlusion abnormalities.The minimum number of animals required for ethical reasons was used in the experiment, and the animals were treated in accordance with the Guiding Opinions on Treating Experimental Animals (Guo ke Fa cai Zi [2006] 398) issued by the Ministry of Science and Technology.The production license number was SCXK (Liao) 2014-0004, and the use license number was SYXK (Liao) 2014-0010. Experimental models of bone defects were used in animal experiments [8]. A completely randomized grouping method was used in this animal study.Group A (n=4) received pure magnesium membrane combined with bone graft material,group B (n=4) received Bio-Gide collagen membrane combined with bone graft material,and control group C (n=4) received only bone graft material (Figure 2).
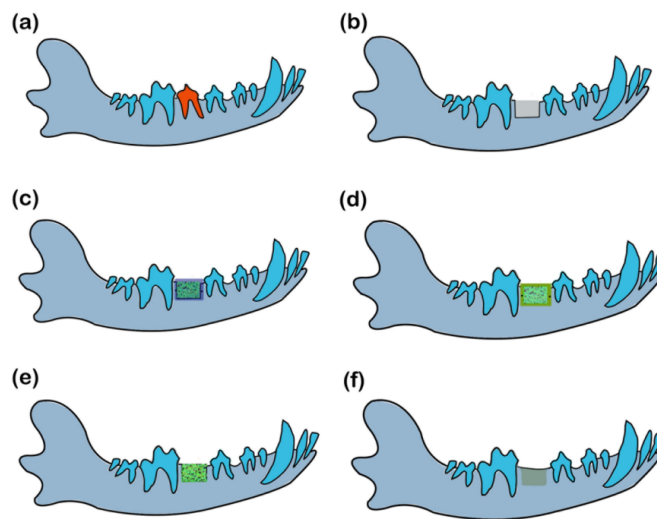
Figure 2: Medical model of vertical mandibular defect in dogs. (a) normal dog mandible, red marked the fourth mandibular premolar. (b) Construct box bone defects area. (c) Group A consisted of a pure magnesium membrane combined with bone graft material.(d)Group B consisted of Bio-Gide collagen membrane combined with bone graft material. (e)Group C served as the control group with bone graft material. (f)Bone healing occurs in the area of the defect.

Surgical Procedures: The experimental animals were deprived of food and water for 12 hours prior to the operation. After weighing the animals, cetirizine hydrochloride (0.1 ml/kg, Jilin Huamu Animal Health Products Co. Ltd, Jilin, China) was injected intramuscularly into their hind legs.After weighing the animals, cetirizine hydrochloride (0.1 ml/kg, Jilin Huamu Animal Health Products Co. Ltd, Jilin, China) was injected intramuscularly into their hind legs.The buccal mucosa was carefully peeled away to expose the mandible's bone surface, and any remaining soft tissue on the bone surface was removed.We then used a dental chisel to remove the bone and produce a box-shaped bone defect model (with dimensions of 10mm length, 6mm width, and 8mm height).A group of four received an implant consisting of a bone graft material combined with a pure magnesium membrane.We trimmed the pure magnesium membrane into a suitable shape according to the size of the bone defect area, ensuring that the edge of the membrane extended beyond the edge of the bone defect by at least 2-3mm. Bio-Gide collagen membrane combined with bone graft material was implanted in group B(n=4), and bone graft material was implanted in group Cas the control group (n=4). Then the pure magnesium film was fixed using magnesium nails. In most cases, the collagen film was firmly wedged under the surrounding mucosa.If this is not feasible, it will be fixed with titanium nails or micro titanium screws in a suitable position. Before covering the membrane, the bone graft material implanted in the bone defect area was compacted and a horizontal mattress suture was used to reduce tension (Figure 3).
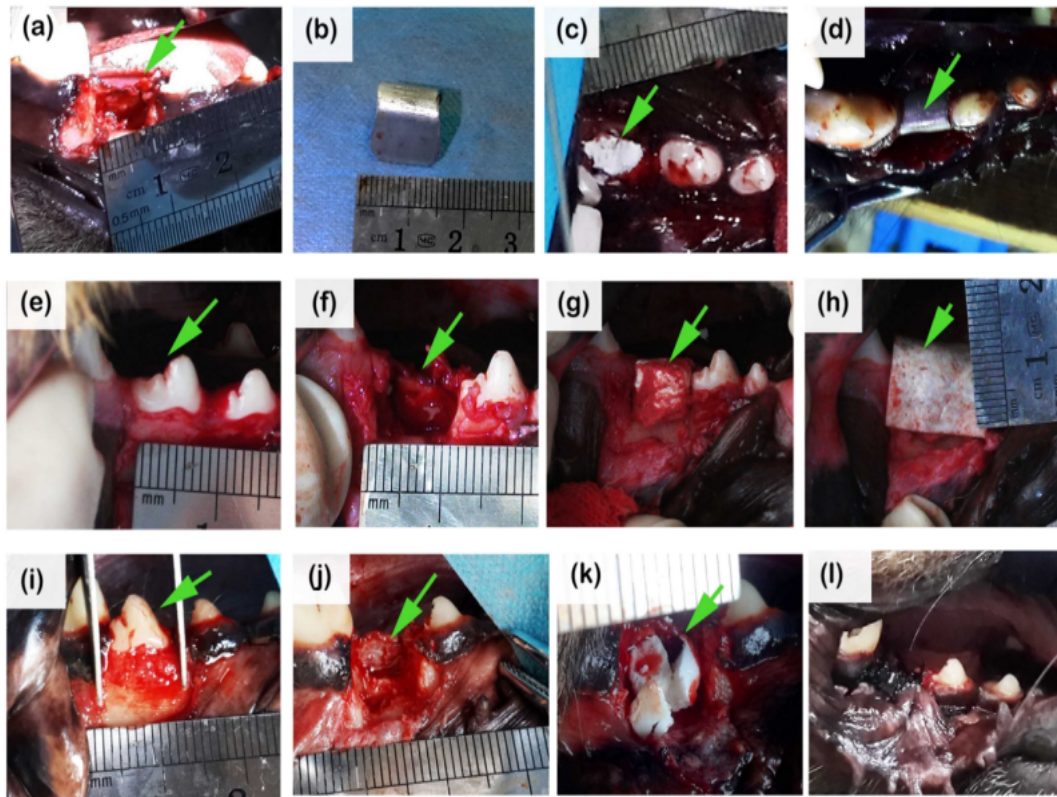

Figure 3: Surgical procedure. Figure (a) The flap was cut open to create a bone defect model. Figure (b) Trim the pure magnesium film into a suitable shape. Figure (c) Place bone graft material. Figure (d) The surface was covered with a pure magnesium film, fixed in place by film nails, and the edges were rounded and blunt. Figures (a)~(d) belonged to group A, while figures (e)~(h) belonged to group B. Figures (a)~(d) belonged to group A, while figures (e)~(h) belonged to group B. Figures (e) to (h) constituted group C, which served as the control group. The bone defect modeling process was similar to group A, but the figure (k) did not include the film.

Postoperative Management: An intramuscular injection of Nikosal (0.08ml/Kg dose) was administered to wake the dogs, and Ampicillin (10mg/Kg, 1 day before surgery, Bar Pharmaceutical Co. Ltd, Sichuan, China) was given three days after surgery to prevent infection.The animals' general condition was observed daily during the implantation cycle while they were being fed.Bleeding, redness, and membrane excretion (magnesium and collagen membranes) at the implantation site were monitored 1, 3, and 5 days after surgery to assess soft tissue reaction in the operative area.

Cone Beam Computed Tomography Analysis: After each animal was anesthetized, it was fixed with a shooting device and scanned using CBCT (Model ProMax 3D, Planmeca, inland). The animals were then observed at 4, 12, and 24 weeks after surgery. The shooting parameters were as follows: tube voltage was 90kV, tube current was 12mA, exposure time was 12.3s, spatial resolution was 2.0lp/mm, pixel size was 0.2mm, imaging range diameter (Φ) was 85mm and height (H) was 75mm.The Romexis Viewer software (version: 2.9.2R, Planmeca, Finland) of the CBCT was utilized for data analysis and exported and saved in DICOM format. The Romexis Viewer software of CBCT was used to conduct three-dimensional measurements.The reconstructed data were as follows: ①Coronal (coronal plane) positioning - the image was adjusted to pass through the near and midline of each dog's left mandibular first molar crown, which connects the mesial and distal crowns (CD-CM). ②Axial(axial plane) positioning: the image was adjusted to pass through the connection line between the apex and root, perpendicular to the coronal plane, and at a distance from the crown tip to root furcation(CT-RF).③Sagittal (sagittal plane) positioning: After determining the two planes, the root bifurcation was positioned perpendicular to both the coronal and axial planes.The sagittal plane was automatically aligned with a specific plane and could not be adjusted.We then adjusted the coronal image to 5mm below the bone junction of the left canine and mandibular first molar tooth crowns, near the middle and middle mandibular teeth.The Romexis software was used to measure the slices The layer thickness was maintained at 2.0mm, and the bone defect area was divided into four coronal sections from mesial to distal.The bone density value was measured in each cross-sectional area of the bone defect repair site, with a measurement range of 1.1 mm² per unit area (Figures 4,5).
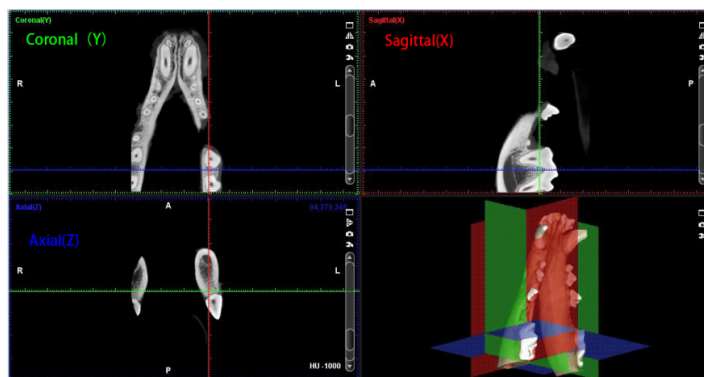
Figure 4: CBCT measurement and positioning. Coronal (Y) positioning, Sagittal (X) positioning, Axial (Z) positioning.
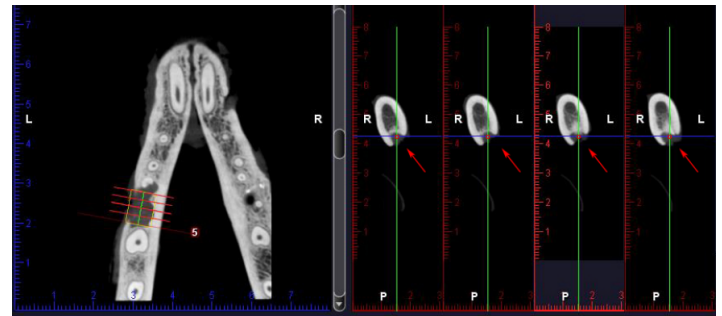
Figure 5: CBCT measurement and positioning. The Romexis software measures the bone density value per unit area of 1.1mm² (indicated by the red circle) in the bone defect repair area, as shown by the red arrow.

X-Ray Microscopic Analysis: Twenty-four weeks after surgery, bone fragments had formed in the area of the dog's mandibular specimen corresponding to the bone defect (measuring 15mm in length, 10mm in width, and 12mm in height). The bone block was placed in an X-ray microscope (X-µCT, Xradia 500 Versa, ZEISS, Germany) and scanned at a voltage of 80 kV, current of 80 µA, and exposure time of 200 ms.Then, using a Scout-and-Scan™ machine control system from ZEISS in Germany,1600 projections were collected during one rotation with a pixel size of 22.4814µm.The data was directly imported into Avizo Fire software (version: Avizo 7, Visualisation Sciences Group, FEI, USA) for 3D visualization and analysis. In the region of bone defect, we selected a Region of Interest (ROI) with a length of 1.18 mm and width of 0.39 mm for three-dimensional reconstruction and observation of trabecular bone structure. A rectangular Volume of Interest area (VOI) with a length of 3032.97µm,width of 1098.90µm, and height of 3842.18µm was selected for analysis based on the ROI.These parameters included bone volume fraction (BV/TV, %) and pore volume fraction (Po, %) of the bone.

Bone Histology Section Observation: The animals were treated in batches at 4, 12, and 24 weeks after surgery, and bone tissue blocks were obtained from the mandibular body surface in both buccal and tongue directions.The bone tissue blocks were placed in a 40g/L paraformaldehyde fixative for 48 hours, rinsed with running water for 24 hours, and dehydrated using a 100% acetone solution in an EXAKT 510 Dehydrator (EXAKT, Germany).The samples were infiltrated with resin using an EXAKT 510 infiltration system for approximately 8 to 10 hours.After dehydration, the bone tissue block is placed into the mould, and the EXAKT E520 (EXAKT, Germany) light curing embedding machine is used for plexiglass

embedding. Tissue sections were produced by polymerizing the organic glass and removing the plastic mold. Technovit 4000 adhesive was used to adhere the organic glass specimens embedded in the slide glass.The upper slide was vacuumed onto a microtome fixture of EXAKT 300 CP (EXAKT, Germany), positioned on the embedded specimen using a laser, and cut the exposed specimen surface with a diamond saw blade. The glass slide was adsorbed onto the EXAKT 400 CS grinding machine to polish the surfaces of the specimens."The Technovit 7210 VLC adhesive was used to attach the lower slide to the polished surface of each specimen using EXAKT 401 slide bonding devices. The upper slides, bone tissue-embedded specimens, and lower slides had a structure similar to that of an Oreo cookie.

Each side of the glass slides was connected to an EXAKT 300CP belt hard tissue cutter. Using an AW100 measurement control system positioning device, each side of the glass slide was gradually sliced into approximately 150 μm thick sections.The slices were then ground. Each side of the glass slides containing the cut bone tissue slices was adsorbed onto the EXAKT 400CS hard tissue grinder, and each ground slice was pre-set to a thickness of 30 μm.It was controlled by the AW100 measurement control system, which used SiC&Al2O3 sandpaper with 800, 1200, and 2000 grain sizes to grind it to a predetermined thickness of 30 μm. A volume fraction of 0.5% toluidine blue staining solution was then directly applied onto the surface of dog mandible slices for 10 to 30 minutes, rinsed under running water, and pathologically mounted after natural drying.

Observation of The Local Soft Tissue Histology of A Pure Magnesium Film: The animals were sacrificed 24 weeks after surgery, and tissues approximately 0.5-1mm surrounding the magnesium membrane were excised.The specimen tissue block was cut into paraffin sections with a thickness of 4 to 5 μm, and the cells were then observed through HE staining.

Histological Observations of Major Organs: Twenty-four weeks after surgery, the heart, liver, spleen, and kidney tissues of each dog were excised and fixed in a 10% neutral formaldehyde solution. The specimen tissue block was cut into paraffin sections with a thickness of 4 to 5 μm, and the cells were then observed through HE staining.

Statistical Analysis

The simplified quantitative data expression is mean±standard deviation, which depends on whether the prerequisites are met and the hypothesis testing method used. Therefore, analysis of variance with a completely random design is employed.If it was unsatisfactory, the Kruskal-Wallis rank sum test would be used. The SPSS 21.0 software package was used for data processing.When $P < 0.05$, the difference between the comparison groups is considered statistically significant, with $\alpha = 0.05$ as the significance level.

Results

Clinical Observation Study

Most of the experimental dogs gradually recovered approximately 40 minutes after surgery, but they remained lethargic and had no appetite. One day after the surgery, the dogs' mucosa in the surgical area was slightly red and swollen, their sutures remained intact, and their mental state had recovered.Three days after surgery, they ate slower than usual due to painful stimulation, and their mucosa was slightly red, but their sutures remained intact. Five days after surgery, the dogs resumed their normal feeding patterns; twelve weeks later, there was no indication that their wounds had extensively split or become infected. An in vitro specimen was observed 24 weeks after surgery. The mucosa in the mandibular surgical regions of group A appeared normal in color, but was tough and elastic compared to the surrounding tissues. The surface mucosa had disintegrated, and partially degraded magnesium nails were observed. The surrounding bone tissues were connected together.The bone tissue was full and contoured. In group B dogs, the mucosa in the mandibular surgical area was normal and firm in color with a relatively clear outline of bone tissue, while at the alveolar crest, it was slightly depressed.The bone tissue outline in the mandibular surgery area of group C was slightly concave, with significantly lower height and width compared to the other groups (Figure 6).
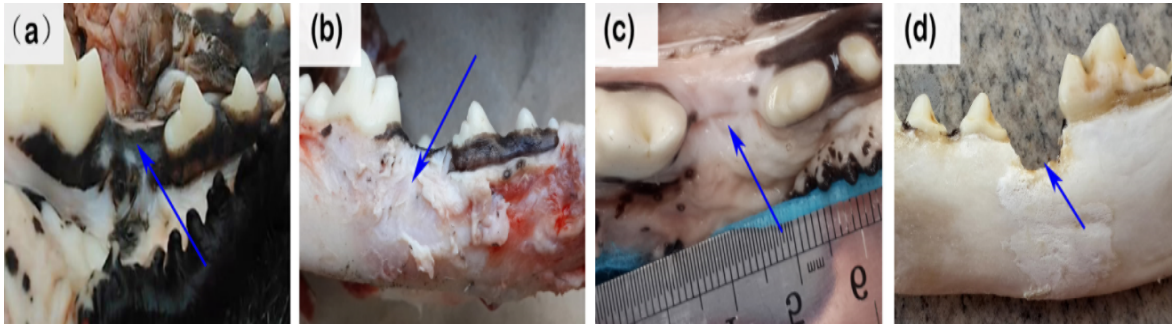
Figure 6: The specimens were observed 24 weeks after surgery. Figures (a) to (b) belonged to group A.The mucosa in the operation area was tough and elastic. The surface mucosa was removed, revealing the full outline of bone tissue.Figure (c) represented group B, and the mucosa corresponding to the crest of the alveolar bone was slightly depressed.Figure (c) represented group B, and the mucosa corresponding to the crest of the alveolar bone was slightly depressed.

Results of Relative Bone Density Measurement Using Cone Beam Computed Tomography

The CBCT results indicated that, 4 weeks after surgery, the image of the osteogenic area inside the magnesium membrane in group A was closer to that of surrounding cancellous bone, but with an unclear boundary.The relative bone mineral density values of groups A and B were higher than that of group C, with statistically significant differences (sig.=0.017,P <0.05). Additionally, there was a statistically significant difference between group A and group B (sig.=0.009, P<0.05).Twelve weeks after surgery, the relative bone mineral density values of groups A and B were higher than those of group C.The difference was statistically significant (sig.=0.013,P<0.05) compared to groups A and B (sig.=0.008,P<0.05). After 24 weeks of surgery, groups A and B showed significantly higher relative bone mineral density values than group C(sig.=0.009, P<0.05). The difference between groups A and B was also statistically significant (sig.=0.010, P<0.05) (Table 1).

Group	4 weeks	12 weeks	24 weeks
Group A	529.78±36.15*Δ	648.51±34.53*Δ	756.59±33.47*Δ
Group B	477.41±32.57*	583.43±37.35*	685.51±32.59*
Group C	421.13±31.49	467.43±34.51	579.61±35.51

Note: Symbols (*) were compared between group A and C,as well as between group B and C. Symbol (Δ) was compared between group A and B, with a significance level of P <0.05.

Table 1: Results of relative bone density measurement using postoperative CBCT (n=4) (x̄±s，unit, HU).

### Results of X-Ray Microscope (XRM) Measurements

Twenty-four weeks after surgery, X-ray microscopy measurements showed that the magnesium film in group A had degraded significantly and the magnesium nails were partially degraded.The magnesium film maintained the internal osteogenic area filled with new trabecular bone and reconstructed it, resulting in thick and dense trabecular bone.The membrane in group B covered the bone defect area, which exhibited signs of new bone formation and many new bone trabeculae. However, the boundary between the bone graft area and surrounding autogenous bone tissue was not clearly defined.The three-dimensional visual trabecular meshwork of Group C is not as tightly arranged as the other two groups, and the boundary between the bone grafting area and surrounding bone tissue is indistinct (Figure 7,8) (Table 2).

| Group	BV/TV	Po
Group A	32.65±0.94*Δ	71.58±3.53*Δ
Group B	29.82±0.85*	65.43±2.95*
Group C	25.57±0.63	59.37±4.17

Note:(*) This symbol indicates that group A was compared with group C, and group B was compared with group C. (Δ) This symbol indicates that group A was compared with group B. BV/TV represents the percentage of trabecular bone volume to the total bone tissue volume.

Table 2: Bone volume fraction (BV/TV, %); Bone pore volume fraction (Po, %), (x̄±s).

The difference in bone volume fraction (BV/TV, %) between groups A and B was statistically significant (sig. = 0.007, $P < 0.05$), as was the difference between group B and group C (sig. = 0.012, $P < 0.05$). There was also a statistically significant difference in the bone pore volume fraction (Po, %) between groups A and B (sig. = 0.017, $P < 0.05$), as well as between groups B and C (sig. = 0.037, $P < 0.05$).
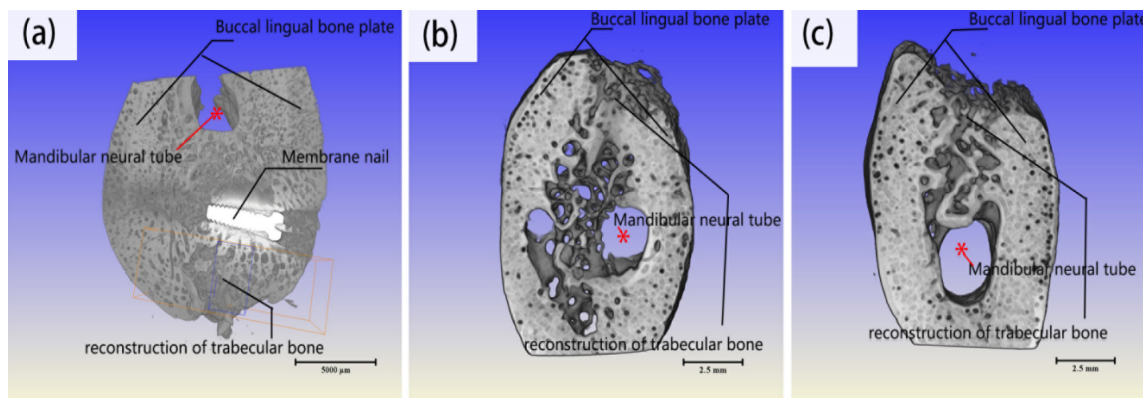
Figure 7: X-ray microscope 3D imaging. Picture (a) represented group A, picture (b) represented group B, and picture (c) represented group C.
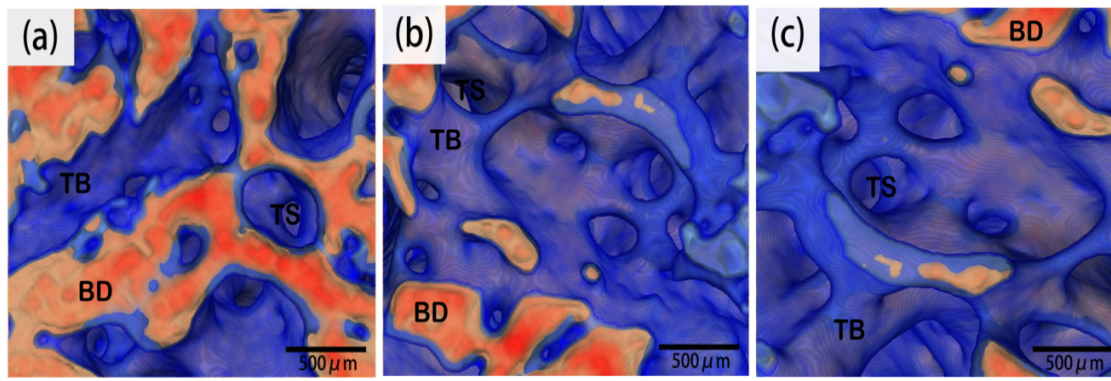
Figure 8: 3D images of the VOI area were taken using an X-ray microscope for each group. Figure (a) shows X-ray microscope images of the VOI region in group A, while figure (b) displays those from group B and figure (c) from group C. The letters BD indicate the boundary, EB indicates trabecular bone, and TS indicates trabecular space.

Observation of Bone Histology Sections

Four weeks after surgery, the magnesium film in group A had partially degraded. The deeply colored irregular crystals around the material indicated exfoliated degradation products and surrounding bone-like tissues.The new bone formed in group B was immature. The original bond with parallel fibers had initiated the initial stage of bone formation, resulting in mainly woven bone. The bone cells were irregularly classified and there was a negligible amount of fibrous tissue present. In group C, which was not covered by the protective membrane, the new bone tissue exhibited some irregularity, loosely arranged trabecular meshwork structure, and visible regrowth of fibrous tissue. Twelve weeks after surgery, the magnesium membrane of group A had degraded concentrically and the magnesium nails had partially degraded. After the woven bone was formed, it penetrated into the trabecular bone space through the bone defect area and filled this original sponge-like scaffold structure. This primitive fibre-parallel bone tissue enhances the sponge-like structure and increases the defect area density. The original primitive spongy scaffold in group B is composed of braided bone, which serves as a template for lamellar bone deposition.In the original sponge-like scaffold, a row of continuous osteoblasts lined the trabecular bone surface, and continuous bone deposition increased the diameter of trabecular bone while reducing the gap between them.The new bone in group C involves bone grafting material. The braided residual bone and bones with parallel fibers were gradually replaced by the lamellar bone bridge, but the trabecular bone was less mature than in the other two groups.

Twenty-four weeks after surgery, the reconstructed bone in group A maintained by the magnesium membrane had reached its final stage of maturity. This led to the formation of absorption lumens through activation of bone metabolic units, which were subsequently refilled with concentric lamellar bone.In group B, there is continuous bone shaping, and osteoblasts and osteoclasts exist on the local bone surface.At the bone modeling site, the number of blood vessels increases, making the trabecular bones more distinguishable and fully connected. In group C, there is a slight maturation in terms of density and structural composition of trabecular bones, with a small amount of visible fibrous tissue remaining (Figure 9).
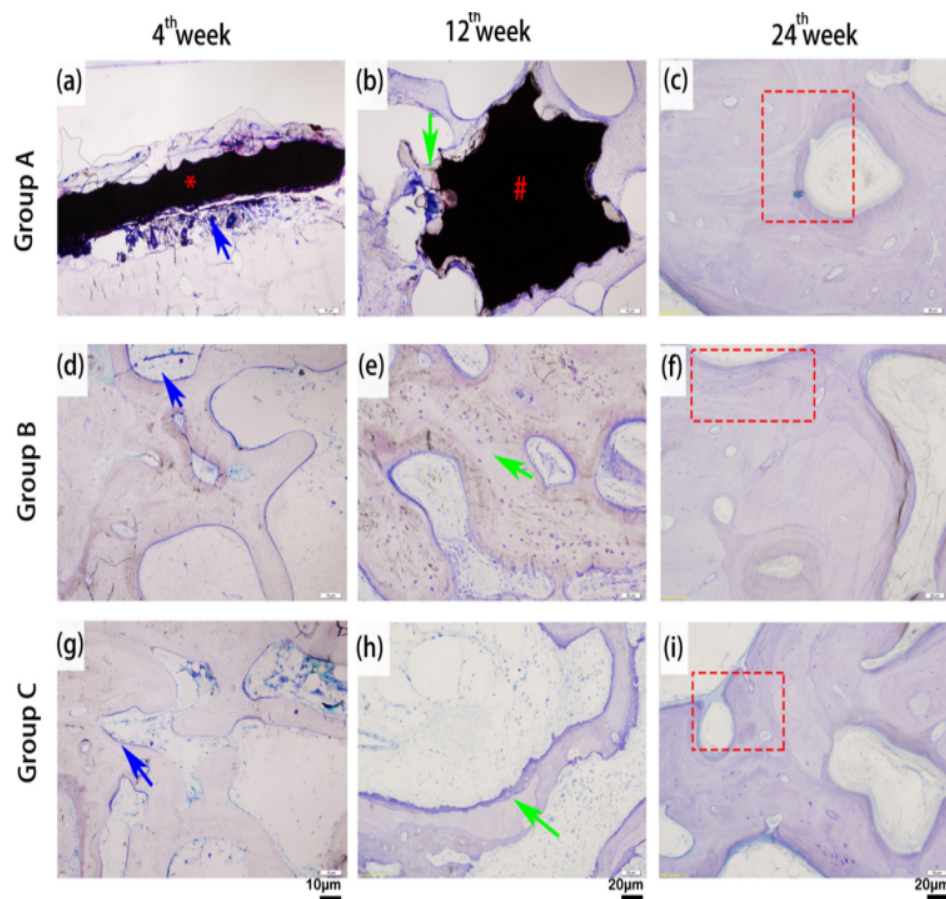
Figure 9: Bone histology section results were obtained for each group with a micro scale of 20 μm. Figures (a)~(c) represent group A, where Figure (a) Symbols (*) indicates degraded magnesium film and the blue arrow points to an irregular crystal-like substance that appears to be exfoliating from the degradation product.Figure (b) indicates the degraded magnesium nails in the area, and the green arrow points to new bone. The red dotted area in Figure (c) shows that bone reconstruction has reached its final stage of maturity. Activation of bone metabolic units leads to formation of absorption lumens, which are subsequently refilled with concentric circular lamellar bone. Figures (d)~(f) belonged to group B. The blue arrow in Figure (d) indicates that the original bones with parallel fibers were deposited in the early stage of bone formation, mainly as woven bones. The green arrow in Figure (e) shows a row of osteoblasts lining the surface of trabecular bone. Continuous bone deposition increases the diameter of trabecular bone and reduces gaps between them.Figure (f) indicates the local presence of osteoblasts, osteocytes, or osteoclasts on the bone surface with a red arrow. Figures (g) to (i) belong to group C. In Figure (g), the blue arrow area shows disordered new bone tissue and trabecular bone structure, as well as obvious fibrous tissue growth.The green arrow in Figure (h) indicates that trabecular bones mature slowly, and the remaining braided bone and bones with fibers arranged in parallel are gradually replaced by lamellar bone. The red area in Figure (i) indicates slow maturation of trabecular bones in terms of density and structure.

Observation of Soft Tissue Sections

The coated mucosa on the surface of the pure magnesium membrane, as well as the epithelial layer and lamina propria, appeared normal with no observed inflammatory reaction. The lamina propria contained a greater number of collagen fiber bundles (Figure 10).
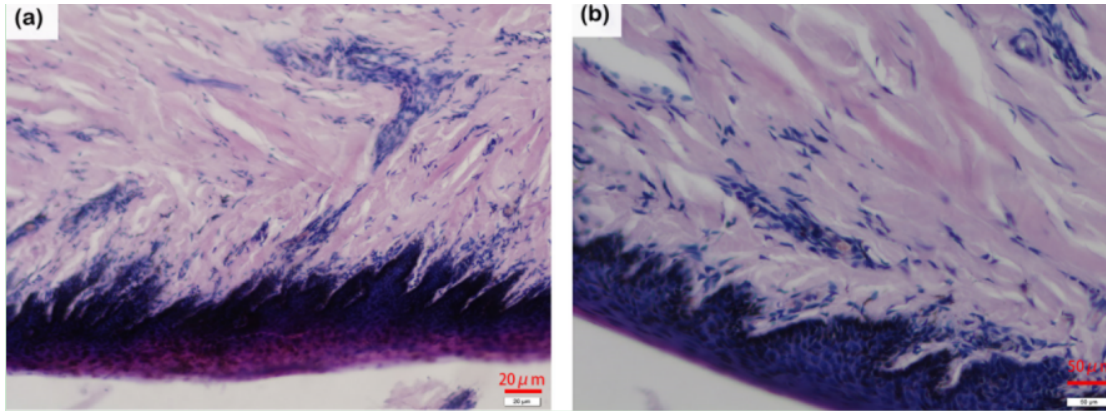

Figure 10: Pure magnesium membrane coated mucosa tissue was stained with HE (hematoxylin and eosin). Figures (a) and (b): No inflammatory reaction was observed in the epithelial layer or lamina propria, but the lamina propria contained more collagen fiber bundles.

In the heart, myocardial fibers are interconnected and intertwined with connective tissue and capillaries between them. The cell nucleus is oval and located approximately in the center of the muscle fiber (Figure 11).
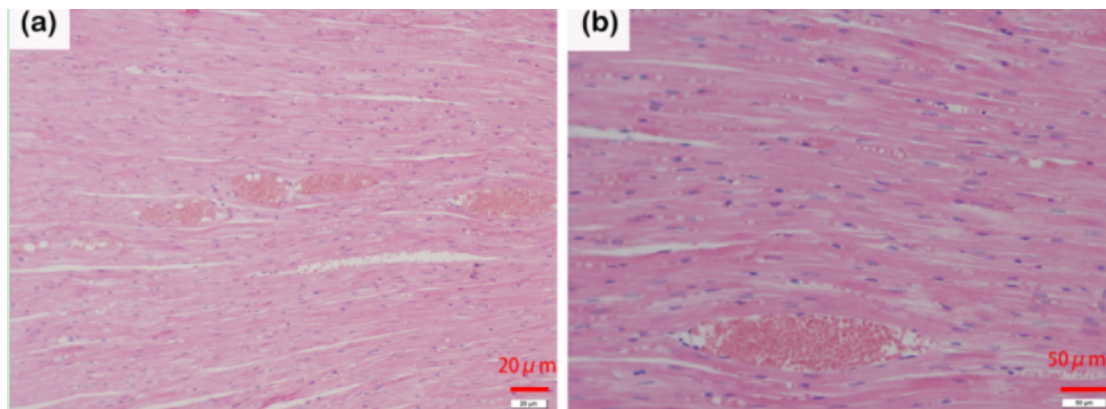
Figure 11: HE stained sections of heart tissue. The red box in Figure (a) indicates that the myocardial fibers were interconnected and intertwined with connective tissue and capillaries in between. The red arrow in Figure (b) indicates an oval-shaped cell nucleus located approximately at the center of the muscle fiber.

In the liver, the interlobular vein and artery structures were normal. The inferior lobular vein was observed in the hepatic lobule, with slightly thicker tube walls (Figure 12).
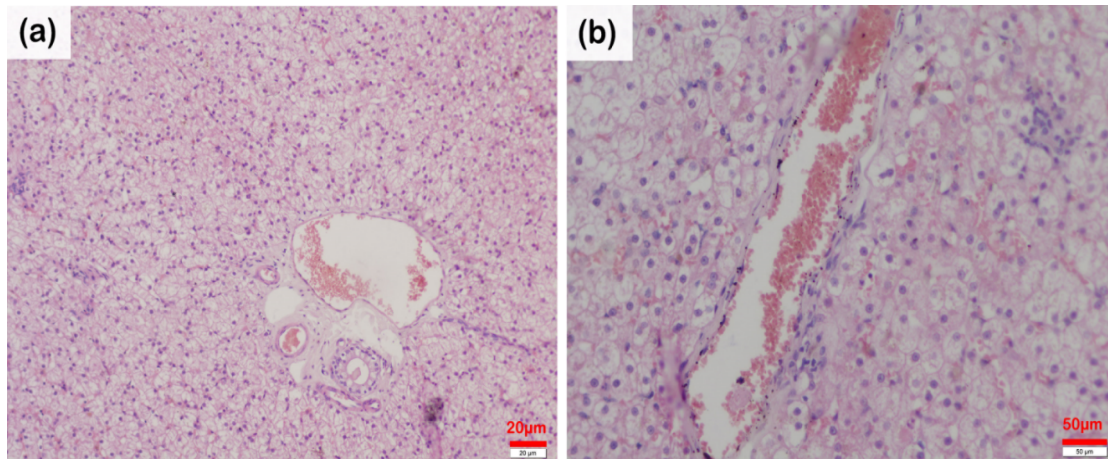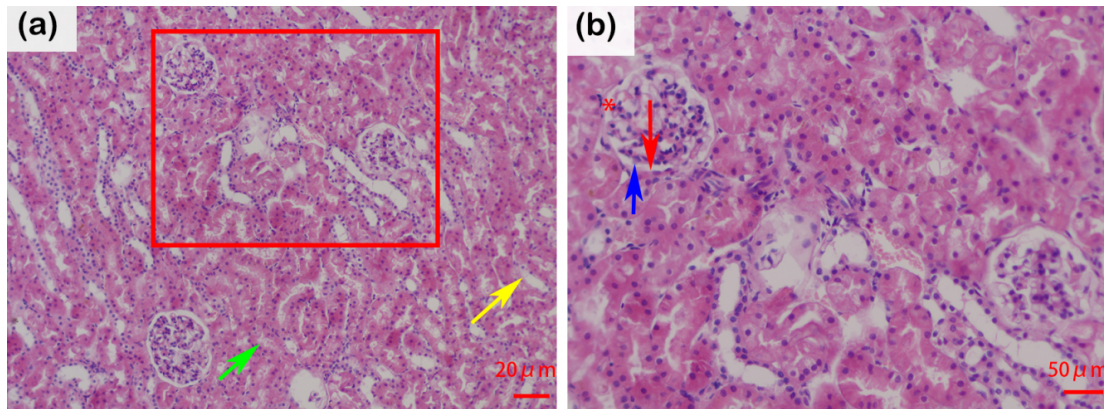
Figure 12: HE stained liver tissue sections. The red box area in Figure (a) indicates that the interlobular artery and vein were normal, while the red arrow area in Figure (b) shows a visible inferior lobular vein with slightly thickened tube wall.

There were no abnormalities in the structures of the splenic sinus and splenic cord in the spleen. The splenic sinus is surrounded by a single layer of cuboidal epithelium (Figure 13).
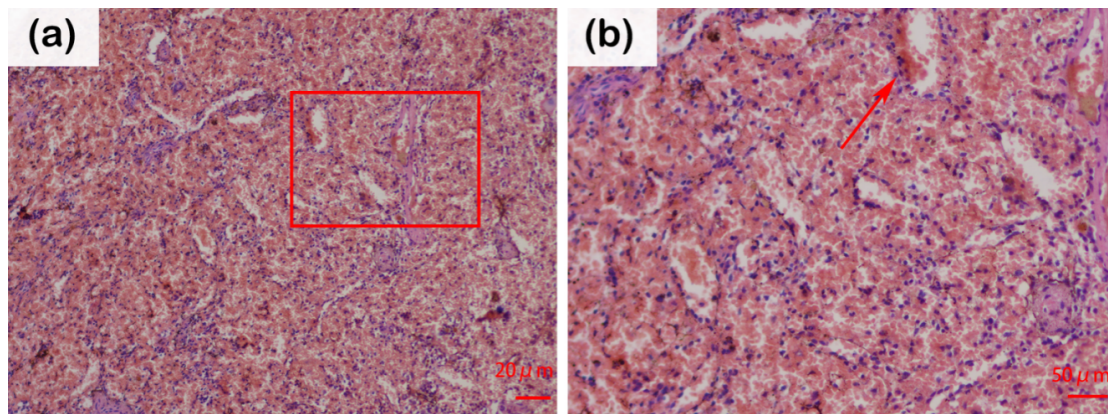
Figure 13: HE stained spleen tissue sections. In Figure (a), the red box area depicts the structure of splenic sinuses and cords. In Figure (b), the red arrow indicates that a single layer of cubic epithelium surrounded the splenic sinus.

In the kidney, the red box area in Figure 14 represents the renal corpuscles, and the green arrow indicates that the proximal lumen is small, irregular, and eosinophilic; while the distal lumen is large and regular. Additionally, cell boundaries are clear and lightly colored (Figure 14).

Figure 14: Kidney tissue sections were HE stained. In Figure (a), the red box area shows the structure of renal corpuscles, where the green arrow indicates a small, irregular proximal lumen with cytoplasmic eosinophilia and the yellow arrow points to a large, regular distal lumen with clear cell boundaries and light coloring.Figure (b): The red arrow indicates that the wall layer of the renal capsule is composed of a single layer of flat epithelium, while the visceral layer is tightly enclosed by the vascular ball (indicated by the blue arrow). Between the viscera and the wall lies the renal capsule cavity (indicated by symbol(*)).

Discussion

The application of shielding membranes is a prerequisite for guided bone regeneration, which creates an environment promoting the advantageous growth of bone tissue by utilizing the different tissue cell migration capabilities and speeds.The shielding membrane is placed between the soft tissue and the bone tissue to establish a biological barrier, creating an isolated space that prevents connective tissue cells and epithelial cells from interfering with bone formation and migrating too quickly into the bone defect area.This enables osteogenic cells with potential for growth and slow migration speeds to preferentially enter the bone defect area and dominate growth. The bone graft material forms a stable scaffold that protects the clot, reduces tissue pressure, maintains space for new bone formation, and achieves repair and complete regeneration of the bone defect area [13,14]. In other words, the shielding membrane creates an isolated space that allows bone tissue to utilize its superior natural healing ability in a protected and interference-free environment.

As research into biological materials has progressed, the performance of the shielding film has continuously improved. Based on the principle and clinical purpose of guided bone regeneration, a shielding film used to guide bone regeneration should possess four basic properties: biocompatibility, cell isolation, maintenance space, and tissue integration [15]. Barrier membranes used to guide bone regeneration can be divided into two categories: bio-inert non-absorbable barrier membranes and bio-absorbable barrier membranes. Bio-inert non-absorbable shielding membranes mainly include materials such as expanded polytetrafluoroethylene (ePTFE), titanium, and micro-porous filter membrane. Currently, there are many animal experiments and clinical applications.The positive effect of guided bone regeneration has been expanded to include tetrafluoroethylene membrane (ePTFE) and titanium membrane, as well as bioabsorbable shielding membranes such as synthetic polyester membranes and animal-derived collagen membranes. Other options include polytechnic acid membranes, polyhydroxyacetate membrane, collagen membranes, and autologous periosteum [16-18]. Among them, commercial products include Bio-Gide (OsteoHealth), BioMend (Galcitech), QsseoQuest (Gore) and others [19]. Expanded tetrafluoroethylene membranes (ePTFE) isolate cells, maintain space, and integrate tissues. However, they are difficult to adhere to the tissue, easily move, and must be fixed with screws and membrane nails which increases surgical time.They are also susceptible to complications such as wound dehiscence, infection, and membrane exposure, which may cause the operation to fail. After new bone forms, a second operation must be performed to remove it, increasing patient pain and expense. Compared with the expanded tetrafluoroethylene membrane, the titanium membrane maintains isolated cells and space. However, due to its lack of tissue integration capabilities, it also has the disadvantages of an expanded tetrafluoroethylene membrane [20]. The advantages of bioabsorbable collagen membranes include good tissue integration and a low risk of membrane exposure. Even if the membrane is exposed to the oral cavity, the rapid degradation of the non-crosslinked collagen membrane is advantageous, and spontaneous re-epithelialization can occur on the wound surface within 2 to 4 weeks.Therefore, there is a low risk of osteogenesis and failure, making secondary surgery to remove the mold unnecessary and reducing the risk of complications. However, due to its poor

stiffness and tendency to collapse, absorbable shielding membranes require joint application with bone graft materials [21-23].

In our observational study of isolated specimens, the experimental dogs in the pure magnesium membrane group had normal-colored mucosa compared to the surrounding tissues, and their texture was tough and elastic. After the surface mucosa was removed, partially degraded magnesium nails integrated with the surrounding bone tissue, and the bone tissue became full and contoured. In the collagen group, the mucosa in dogs' mandibular surgical area appeared normal and firm in color, and the outline of bone tissue was relatively complete. In the control group, the bone tissue outline in the dogs' mandibular surgical area was slightly concave, and both its height and width were significantly lower than those in the other two groups.

Literature reports indicate that CBCT has the advantages of high spatial resolution, relatively low radiation dose, and good three-dimensional imaging of hard tissue structures. Therefore, it is widely used in both basic oral and clinical research [24]. In reconstructed CT images, each CT value corresponds to a greyscale representation that demonstrates the tissue density of each pixel. The varying CT values create differences in greyscale within the CT images. Reports indicate that CBCT greyscale values remain consistent across different exposure times and doses. The degree of X-ray attenuation in CBCT is represented by voxels in greyscale. In other words, CBCT grayscale can be used to estimate bone density [25]. The cone-beam CT results of the current study showed that groups A and B had higher relative bone mineral density values than group C at 4, 12, and 24 weeks after surgery. The difference between groups A and B was statistically significant, which demonstrates that pure magnesium film possesses both mechanical and metallurgical properties, as well as good space maintenance ability.

In the guided bone tissue regeneration process, new trabecular bone often objectively reflects the condition of bone healing. The structural changes in trabecular bone largely reflect the effect of osteogenesis [26]. X-ray microscope measurements show that the pure magnesium film is basically degraded and the magnesium nail is partially degraded. The magnesium membrane maintains the internal osteogenic area filled with new bone trabeculae and completes the reconstruction. The bone trabeculae are thick and dense, and the collagen membrane covering the bone defect area shows signs of new bone formation with many new bone trabeculae present. The boundary between the bone grafts area and surrounding autogenous bone tissue is not clearly defined. The trabecular meshwork structure of the control group was not as tightly ordered as those of the other two groups, and the boundary between the bone grafting area and surrounding bone tissue was indistinct. The results showed that the pure magnesium membrane

group had a higher bone volume fraction than both collagen membrane and control groups, with statistically significant differences. The pure magnesium membrane group had a higher bone pore volume fraction than the collagen membrane and control groups, and the difference was statistically significant. This suggests that pure magnesium membranes play a significant role in guiding bone tissue regeneration. Additionally, pure magnesium membranes have an advantage over collagen membranes in preventing collapse.

The EXAKT bone tissue cutting and grinding system is capable of producing high-quality cortical bone and metal-containing implant bone slices [27]. Toluidine blue staining is particularly suitable for observing the staining of bone tissue, especially in studies related to bone tissue reconstruction. This method is beneficial for observing newly mineralized bone and original lamellar bone in a bone defect, which helps repair the corresponding area in bone morphometry measurements. The experimental results showed that the magnesium membrane group had partially degraded after four weeks. Deeply colored irregular crystals in the material indicated the presence of degraded exfoliated products, and bone-like tissues were observed in the magnesium film. The release of magnesium ions during degradation of the film created a microenvironment within the bone tissue covered by the film, which increased levels of Bone Morphogenetic Protein (BMP-2) and promoted local new bone formation [28] (Figure 15).
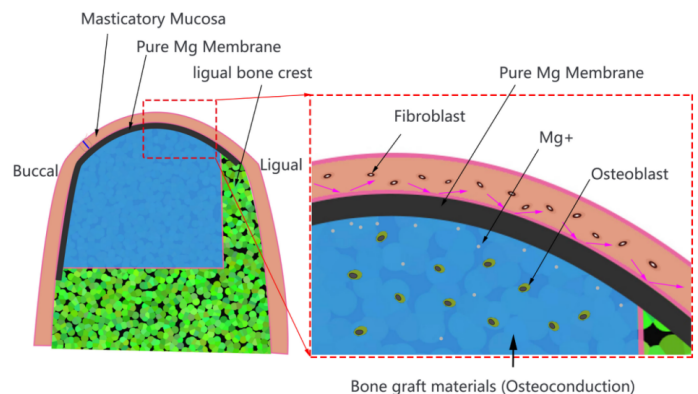
Figure 15: Pure magnesium membrane guided bone regenerative medicine model diagram. In the repair of bone defects, the pure magnesium membrane is used to maintain space for bone regeneration, preventing epithelial cells and fibroblasts from entering the bone defect area. This allows slow growth of blood vessels and bone cells to enter the affected area.

The shielding membrane maintains the internal space and clearly isolates it from the external structure composed of oral mucosa, so that the internal space is not affected by the bone

marrow cavity. At this time, the internal space mainly consists of regenerated spongy bone, and the bone marrow trabecula forms slender and blurred cavities.The bone marrow cavity is rich in loose connective tissue and blood vessels, and the blood vessels and fibrous tissue continue around the defect. Primitive spongy branches then form. The histological performance of bone formation in the space maintained by the shielding membrane is surprisingly similar to that of bone growth and development [29,30]. Blood vessels and bone-forming cells invade the blood clot and a braided bone scaffold. During the progressive osteogenesis process, the blood vessels tightly combine with the formed bone trabeculae. The original primitive spongy scaffold consisted of braided bone, and in the early stage of bone formation, primordial bones with fibers arranged in parallel had deposits of braided bones.The irregular arrangement of cells in the bone serves as a template for lamellar bone deposition, which eventually forms dense bone with mature bone marrow and regular cancellous bone [31-33]. These changes occur 12 to 16 weeks after surgery, and the results of the experimental study are consistent with them. The experimental results show that the surface of the trabecular bone in the original spongy scaffold is lined with a row of continuous osteoblasts, and successive bone deposition increases the diameter of the trabecular bone while reducing the gap between its components.The woven bone in the newly formed bone transforms into lamellar bone, and bones with parallel fibers demonstrate a transitional stage in this maturation process. The maturation process terminates when the space between trabecular bones reaches the normal diameter of the central canal, and concentric circular laminar bone surrounding it constitutes the primary unit of bone.The formation of secondary or regular cancellous bone begins at the center of the bone defect, and the bone marrow cavity expands due to absorption of the original sponge scaffold. Experimental results demonstrate complete reconstruction of remaining trabecular bones, with gradual replacement of remaining woven and parallel-fibered bones by a lamellar bone bridge.This process also begins at the periphery and progresses towards the center of the bone defect, resulting in cancellous bone that is connected to the pre-existing trabecular bone surrounding the defect.

The experimental results show that bone reconstruction in the space maintained by the magnesium membrane reaches its final stage of maturity 24 weeks after surgery. The activation of bone metabolic units leads to the formation of absorption lumens, which are subsequently refilled with concentric lamellar bone. The collagen membrane group also underwent continuous bone shaping, and osteoblasts, osteoid-like layers, or osteoclasts were locally present on the bone surface. In the control group without a shielding membrane, bone formation was limited to the edge of the bone defect because there was no shielding membrane covering it.After 12 weeks, the marrow cavity had closed, but there was

no improvement in bone formation. By week 16, there was a slight increase in bone density and trabecular bone maturation showed low density and structural composition with some visible fibrous tissue remaining. The effect of the pure magnesium film on the oral mucosa around the implantation site was evaluated to determine hydrogen release and local alkaline environment during degradation of the film.The experimental results showed that the mucosa coated on the surface of the pure magnesium membrane, including the epithelial layer and lamina propria, was normal with no observed inflammatory reactions. Additionally, more collagen fiber bundles were present in the lamina propria.

Whether pure magnesium film is the superior shielding film that can eventually be used as a guided bone regeneration material for clinical applications remains unclear, thus further research is necessary.Our research group intends to study the following factors: surface modification of pure magnesium and magnesium alloy shielding film materials; structural integrity in a specific physiological animal environment during degradation; mechanical strength and other properties with service time law of degradation; controllable degradation mechanism and ion release kinetic characteristics, etc.

Conclusions

Pure magnesium film has the mechanical properties of metals and biodegradability, as well as superior space maintenance. The pure magnesium membrane possesses a certain level of mechanical strength that is similar to natural bone, which can guide and control the outline of regenerated bone. Additionally, it avoids the issue of collagen membranes collapsing and better maintains space for bone regeneration in larger defects.

Funding

References

1. Mendoza-Azpur G, de la Fuente A, Chavez E, Valdivia E, Khouly I (2019) Horizontal ridge augmentation with guided bone regeneration using particulate xenogenic bone substitutes with or without autogenous block grafts: A randomized controlled trial. Clin Implant Dent Relat Res 21: 521-530.

2. Sábado-Bundó H, Sánchez-Garcés MÁ, Gay-Escoda C (2019) Bone regeneration in diabetic patients. A systematic review. Med Oral Patol Oral Cir Bucal 24: 425-432.

3. Elgali I, Omar O, Dahlin C, Thomsen P (2017) Guided bone regeneration: materials and biological mechanisms revisited. Eur J Oral Sci 125: 315-337.

4. Cucchi A, Sartori M, Parrilli A, Aldini NN, Vignudelli E, et al. (2019) Histological and histomorphometric analysis of bone tissue after guided bone regeneration with non-resorbable membranes vs resorbable membranes and titanium mesh. Clin Implant Dent Relat Res 21: 693-701.

5. Cucchi A, Vignudelli E, Napolitano A, Marchetti C, Corinaldesi G (2017) Evaluation of complication rates and vertical bone gain after guided bone regeneration with non-resorbable membranes versus titanium meshes and resorbable membranes. A randomized clinical trial. Clin Implant Dent Relat Res 19: 821-832.

6. Kamrani S, Fleck C (2019) Biodegradable magnesium alloys as temporary orthopaedic implants: a review. Biometals 32: 185-193.

7. Hung CC, Chaya A, Liu K, Verdelis K, Sfeir C (2019) The role of magnesium ions in bone regeneration involves the canonical Wnt signaling pathway. Acta Biomater 98: 246-255.

8. Zhang S, Sun X, Kang C, Yang M, Zhao Y, et al. (2020) Study on repairing canine mandibular defect with porous Mg-Sr alloy combined with Mg-Sr alloy membrane. Regen Biomater 7: 331-336.

9. Yu Q, Wang C, Yang J, Guo C, Zhang S (2018) Mineralized collagen/Mg-Ca alloy combined scaffolds with improved biocompatibility for enhanced bone response following tooth extraction. Biomed Mater 13: 065008.

10. Yang J, Koons GL, Cheng G, Zhao L, Mikos AG, et al. (2018) A review on the exploitation of biodegradable magnesium-based composites for medical applications. Biomed Mater 13.

11. Guo C, Yu Q, Sun BZ, Wang CY, Yang JX (2018) Evaluation of Alveolar Bone Repair with Mineralized Collagen Block Reinforced with Mg–Ca Alloy Rods. J Biomater Tiss Eng 8: 1-10.

12. Sun XR, Wang CY, Zhao Y, Zhang ZB (2020) In vitro corrosion and in vivo biosafety of pure magnesium film. Zhongguo Zuzhi Gongcheng Yanjiu 24: 2578-2584.

13. Urban IA, Monje A (2019) Guided Bone Regeneration in Alveolar Bone Reconstruction. Oral Maxillofac Surg Clin North Am 31: 331-338.

14. Arunjaroensuk S, Panmekiate S, Pimkhaokham A (2018) The Stability of Augmented Bone Between Two Different Membranes Used for Guided Bone Regeneration Simultaneous with Dental Implant Placement in the Esthetic Zone. Int J Oral Maxillofac Implants 33: 206-216.

15. Wang HL, Boyapati L (2006) "PASS" principles for predictable bone regeneration. Implant Dent 15: 8-17.

16. Soldatos NK, Stylianou P, Koidou VP, Angelov N, Yukna R, et al. (2017) Limitations and options using resorbable versus nonresorbable membranes for successful guided bone regeneration. Quintessence Int 48: 31-147.

17. Cao YB, Liu C, Pan WL, Tu Y, Li CJ, et al. (2019) Research progress on the modification of guided bone regeneration membranes. Hua Xi Kou Qiang Yi Xue Za Zhi 37: 325-329.

18. Garcia J, Dodge A, Luepke P, Wang HL, Kapila Y, et al. (2018) Effect of membrane exposure on guided bone regeneration: A systematic review and meta-analysis. Clin Oral Implants Res 29: 328-338.

19. Amoian B, Moudi E, Majidi MS, Ali Tabatabaei SM (2016) A histologic, histomorphometric, and radiographic comparison between two complexes of CenoBoen/CenoMembrane and Bio-Oss/Bio-Gide in lateral ridge augmentation. A clinical trial. Dent Res J (Isfahan) 13: 446-453.

20. Schneider D, Weber FE, Grunder U, Andreoni C, Burkhardt R, et al. (2014) A randomized controlled clinical multicenter trial comparing the clinical and histological performance of a new, modified polylactide-co-glycolide acid membrane to an expanded polytetrafluoroethylene membrane in guided bone regeneration procedures. Clin Oral Implants Res 25: 150-158.

21. Naung NY, Shehata E, Van Sickels JE (2019) Resorbable Versus Nonresorbable Membranes: When and Why? Dent Clin North Am 63: 419-431.

22. Brignardello-Petersen R (2018) Membrane exposure may decrease the benefits of guided bone regeneration on bone levels in the short term. J Am Dent Assoc 149: 119.

23. Lindfors LT, Tervonen EA, Sándor GK, Ylikontiola LP (2010) Guided bone regeneration using a titanium-reinforced ePTFE membrane and particulate autogenous bone: the effect of smoking and membrane exposure. Oral Surg Oral Med Oral Pathol Oral Radiol Endod 109: 825-830.

24. EzEldeen M, Wyatt J, Al-Rimawi A, Coucke W, Shaheen E, et al. (2019) Use of CBCT Guidance for Tooth Autotransplantation in Children. J Dent Res 98: 406-413.

25. Gardner SJ, Mao W, Liu C, Aref I, Elshaikh M, et al. (2019) Improvements in CBCT Image Quality Using a Novel Iterative Reconstruction Algorithm: A Clinical Evaluation. Adv Radiat Oncol 4: 390-400.

26. De Santis D, Sinigaglia S, Pancera P, Faccioni P, Luciano U, et al. (2019) An overview of guided bone regeneration. J Biol Regul Homeost Agents 33: 49-53.

27. Ripamonti U, Roden LC, Renton LF (2012) Osteoinductive hydroxyapatite-coated titanium implants. Biomaterials 33: 3813-3823.

28. Cheng P, Han P, Zhao C, Zhang S, Wu H, et al. (2016) High-purity magnesium interference screws promote fibrocartilaginous entheses regeneration in the anterior cruciate ligament reconstruction rabbit model via accumulation of BMP-2 and VEGF. Biomaterials 81: 14-26.

29. Dimitriou R, Jones E, McGonagle D, Giannoudis PV (2011) Bone regeneration: current concepts and future directions. BMC Med 9: 66.

30. Stricker A, Fleiner J, Stübinger S, Fleiner H, Buser D, et al. (2016) Ridge preservation after ridge expansion with simultaneous guided bone regeneration: a preclinical study. Clin Oral Implants Res 27: e116-e124.

31. Jung RE, Herzog M, Wolleb K, Ramel CF, Thoma DS, et al. (2017) A randomized controlled clinical trial comparing small buccal dehiscence defects around dental implants treated with guided bone regeneration or left for spontaneous healing. Clin Oral Implants Res 28: 348-354.

32. Gut G, Ambroziak M, Bojar W, Szaraniec B, Chłopek J, et al. (2018) *In Vitro* and *in Vivo* (Rabbit, Guinea Pig, Mouse) Properties of a Novel Resorbable Polymer and Allogenic Bone Composite for Guided Bone Regeneration and Orthopedic Implants. Transplant Proc 50: 2223-2228.

33. Al-Hezaimi K (2016) Real-Time Assessment of Osseous Tissue Changes After Guided Bone Regeneration. Int J Periodontics Restorative Dent 36: s7-s8.